Open Research Online

The Open University's repository of research publications
and other research outputs

Field-free spin-orbit torque switching of a perpendicular ferromagnet with Dzyaloshinskii-Moriya interaction

Journal Item

How to cite:

Chen, BingJin; Lourembam, James; Goolaup, Sarjoosing and Lim, Sze Ter (2019). Field-free spin-orbit torque switching of a perpendicular ferromagnet with Dzyaloshinskii-Moriya interaction. Applied Physics Letters, 114(2), article no. 022401.

For guidance on citations see FAQs.

© 2019 The Authors

Version: Version of Record

Link(s) to article on publisher's website:
http://dx.doi.org/doi:10.1063/1.5052194

Copyright and Moral Rights for the articles on this site are retained by the individual authors and/or other copyright owners. For more information on Open Research Online's data policy on reuse of materials please consult the policies page.

oro.open.ac.uk

Applied Physics Letters

Field-free spin-orbit torque switching of a perpendicular ferromagnet with Dzyaloshinskii-Moriya interaction

Cite as: Appl. Phys. Lett. **114**, 022401 (2019); https://doi.org/10.1063/1.5052194
Submitted: 14 August 2018 . Accepted: 22 December 2018 . Published Online: 15 January 2019

BingJin Chen, James Lourembam, Sarjoosing Goolaup, and Sze Ter Lim

View Online Export Citation CrossMark

ARTICLES YOU MAY BE INTERESTED IN

Ultrafast field-free magnetization switching using bi-directional spin Hall current and antiferromagnetic interlayer exchange
Applied Physics Letters **114**, 012403 (2019); https://doi.org/10.1063/1.5063423

Spin-orbit-torque-driven multilevel switching in Ta/CoFeB/MgO structures without initialization
Applied Physics Letters **114**, 042401 (2019); https://doi.org/10.1063/1.5079313

High-speed STT MRAM incorporating antiferromagnetic layer
Applied Physics Letters **114**, 022403 (2019); https://doi.org/10.1063/1.5078525

AIP Publishing

© 2019 Author(s).

Applied Physics Letters ARTICLE scitation.org/journal/apl

Field-free spin-orbit torque switching of a perpendicular ferromagnet with Dzyaloshinskii-Moriya interaction

Cite as: Appl. Phys. Lett. **114**, 022401 (2019); doi: 10.1063/1.5052194
Submitted: 14 August 2018 · Accepted: 22 December 2018 · Published Online: 15 January 2019

View Online Export Citation CrossMark

BingJin Chen,[a] James Lourembam, Sarjoosing Goolaup, and Sze Ter Lim

AFFILIATIONS

Institute of Materials Research and Engineering (IMRE) Agency for Science, Technology and Research (A*STAR), 2 Fusionopolis Way, Innovis, #08-03, Singapore 138634

[a] Author to whom correspondence should be addressed: Chen_BingJin@imre.a-star.edu.sg

ABSTRACT

Leveraging on interfacial Dzyaloshinskii-Moriya interaction (DMI) induced intrinsic magnetization tilting in nanostructures, a parametric window enabling field-free spin-orbit torque (SOT) magnetization switching in a perpendicular ferromagnet is established. The critical current density (J_c) bounds for SOT switching are highly dependent on the DMI, producing a distorted diamond-shaped region bounded by the J_c-DMI curves. The widest J_c interval is found for DMI values between 0.5 mJ/m^2 and 0.8 mJ/m^2. Geometrical modulation, of the ferromagnetic layer, reveals that the circular structure is optimum for minimizing the switching energy while maximizing the parametric window. For all the structures investigated, the SOT induced reversal process is *via* domain wall nucleation and propagation, and the switching is practical at room temperature.

Published under license by AIP Publishing. https://doi.org/10.1063/1.5052194

Spin-transfer torque magnetic random access memory is a promising emerging memory technology because of its non-volatility, fast access time, high endurance, as well as zero standby power.[1–5] However, a high write current passing through the magnetic tunnel junction (MTJ) may deteriorate the tunnel barrier; the read current could also cause read disturbance errors since the read and the write operations share the same current path.[6,7] Spin-orbit torque magnetic random access memory (SOT-MRAM) can overcome these limitations *via* a three-terminal device wherein the write and read current paths are decoupled[8–10] [Fig. 1(a)]. However, to date, deterministic SOT induced switching of a perpendicular magnetization requires an external magnetic field, which is a major challenge for practical realization of devices.[11–16] To realize field-free SOT switching of a perpendicular magnetization, alternative methods have been proposed, such as using structures with broken lateral inversion symmetry,[17,18] engineering a tilted anisotropy,[19] and the assistance of an antiferromagnetic layer (AFM).[20–22] However, all these schemes require complicated structures and often compromise the thermal stability of the MTJs.

SOT arises from the strong spin-orbit coupling and the broken structural inversion symmetry at the ferromagnet (FM)/heavy metal (HM) interface. Incidentally, the spin-orbit coupling at the interface leads to chiral interactions, Dzyaloshinskii-Moriya interaction (DMI), appearing at the FM/HM interface.[23–28] The effect of DMI on SOT switching has been studied recently both experimentally[29–31] and through micromagnetic simulations.[32–35] DMI can induce non-uniform magnetization textures of a definite chirality and significantly affects the magnetization reversal process. However, a detailed study on exploring the full range of DMI parameters to induce field-free SOT switching is still lacking.

Here we perform micromagnetic simulations using the Object Oriented Micro-Magnetic Framework (OOMMF) public code[36] by numerically solving the Landau-Lifshitz-Gilbert-Slonczewski (LLGS) equation with DMI terms[37] (see supplementary material).

We use the following parameters in the simulations: exchange constant, $A = 2 \times 10^{-11}$ J/m, saturation magnetization of the free layer, $M_s = 1100 \times 10^3$ A/m, intrinsic perpendicular anisotropy of the free layer, $K_U = 0.8$ MJ/m^3, the damping constant $\alpha = 0.1$, and the spin Hall angle $\alpha_H = 0.3$. The free layer is assumed to be circular with a diameter of 100 nm and is discretized into 2 nm × 2 nm × 1.1 nm for calculations.

Published under license by AIP Publishing

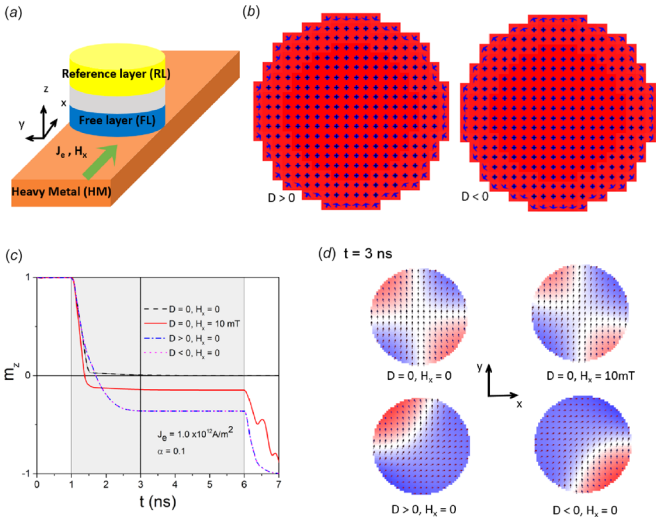

FIG. 1. DMI induced field-free spin-orbit torque switching: (a) sketch of an SOT-MRAM cell structure based on a top-pinned MTJ; (b) snapshots of magnetization profiles at 1 ns (magnetization states after relaxation) for $D > 0$ and $D < 0$; (c) temporal evolutions of the perpendicular magnetization component under various D and H_x conditions (the pulse is applied within the shaded region). The vertical line at $t = 3$ ns indicates the critical configuration; (d) snapshots of magnetization profiles at 3 ns corresponding to the input conditions of (c).

To understand the effect of DMI and in-plane external magnetic field (H_x) on SOT switching separately and in combination, we perform micromagnetic simulations for the following parametric cases: (i) $D = 0, H_x = 0$; (ii) $D = 0, H_x \neq 0$; (iii) $D > 0, H_x = 0$; and (iv) $D < 0, H_x = 0$. The results detailed in Fig. 1 are for up (↑) to down (↓) magnetization switching. In our simulations, the initial magnetization configuration of the device is set for $m_z = 1$ and relaxed for 1 ns before applying a current pulse of amplitude $J_e = 1.0 \times 10^{12} A/m^2$ and width $t_p = 5$ ns.

Snapshots of magnetization profiles at $t = 1$ ns (magnetization states after relaxation) from our simulations due to a finite interfacial DMI ($D \neq 0$) are shown in Fig. 1(b). The local magnetization at the edges tilts inwards into (outwards from) the center of the free layer for $D > 0$ ($D < 0$). This is due to the fact that interfacial DMI imposes boundary conditions at the edge of the ferromagnet.[37] In practice, the sign of D can be reversed by inverting the stack structure.

Figure 1(c) shows the simulated temporal evolution of the out-of-plane magnetization component, m_z, for all four cases. Within 1 ns ($t = 2$ ns) from the pulse onset, the m_z component approaches or crosses over 0, resulting in a critical magnetization configuration at $t = 3$ ns. Interestingly, for $H_x > 0$ (ii) or $D \neq 0$ (iii and iv), the critical m_z component adopts a negative value.

For case (i), m_z approaches 0, which leads to a non-deterministic state if the current is removed. This is consistent with the results from previous macrospin simulations.[38] In perpendicular magnets, two stable states are present without current, up and down. Under SOT, these states are displaced and even merge at a sufficiently high current density (J_e), around a point defined by $m_z = 0$ and $m_y = \pm 1$ depending on current polarity if $D = 0$ and $H_x = 0$. For this reason, switching this way is usually stochastic because relaxation upon removing the current can proceed to either up or down state. On the other hand, introducing an in-plane field of $H_x = 10$ mT, case (ii), assists m_z to cross over the zero axis leading to deterministic switching. This is the well-known mechanism of achieving deterministic SOT switching. Interestingly, DMI plays a similar role to the in-plane field in aiding the m_z to shift into the negative region, as in cases (iii) and (iv). It is shown that the presence of DMI forbids to have exact $m_z = 0$, but instead $m_z > 0$ or $m_z < 0$ (depending on the initial magnetization), during the pulse. As a consequence, when the pulse ends, relaxation from this displaced equilibrium proceeds, and depending on the history of the dynamics, relaxation can lead to a given, reproducible final state for a particular (D, J_e) combination. At appropriate current densities, and for suitable values of D, it shown that the final state is always opposite to the initial, that is, switching is achieved. We note here that our micromagnetic simulations have an essential difference with macrospin simulations, which cannot consider the effect of D. Indeed, the switching dynamics relies on a non-uniformity of the magnetization. Based on the drop in m_z below 0, the effect of $D = 0.5$ mJ/m^2 is equivalent to an in-plane field of $H_x = 28$ mT for $D = 0$.

Figure 1(d) depicts the snapshots of magnetization configurations at time $t = 3$ ns during the current pulse for all four cases. The final state at the end of the pulse is already determined by the magnetization state at 3 ns. In the absence of both DMI and in-plane field ($D = 0, H_x = 0$), the magnetizations go in-plane [Fig. 1(d), top-left], resulting in non-deterministic switching once the current is removed. That is, the magnetization, m_z, has equal probability of returning to its initial state or switching to the opposite state. With the assistance of an in-plane field ($D = 0, H_x \neq 0$), the symmetric magnetization pattern is broken [Fig. 1(d) top-right], resulting in deterministic switching. On the other hand, introducing DMI into the system ($D > 0, H_x = 0$ or $D < 0, H_x = 0$) can be another approach to induce magnetization asymmetry [Fig. 1(d) bottom-left and bottom-right] and may eventually lead to field-free deterministic switching. Here, the sign of the DMI only affects the chirality of the in-plane magnetization configuration nucleated within the structure. Positive (negative) D induces anti-clockwise (clockwise) in-plane magnetization rotations [Fig. 1(d)]. The collective magnetization reversal process is identical for opposite DMI signs as shown in Fig. 1(c). In all the cases investigated above, we did not observe coherent reversal of magnetization.

We now conduct systematic investigation on the combined effect of DMI and current density on the magnetization switching performance. The results are illustrated in Fig. 2. During the simulations, the device is initially relaxed for 1 ns before a current with a pulse width of $t_p = 5$ ns is applied.

Figures 2(a) and 2(b) are plots of temporal evolutions of magnetization components (m_x, m_y, m_z) at a current density $J_e = 1.0 \times 10^{12}$ A/m^2 for up (↑) to down (↓) magnetization switching and *vice-versa*, respectively. It is shown that the same current polarity can switch the magnetizations both from up (↑) to down (↓) and vice-versa. This indicates that DMI induced field-free switching is unipolar in nature. Figures 2(c) and 2(d) display the temporal evolutions of perpendicular magnetization

Published under license by AIP Publishing

component m_z with $D = 0.5\ mJ/m^2$ for various current densities ranging from $J_e = 0.82 \times 10^{12} A/m^2$ to $J_e = 1.1 \times 10^{12} A/m^2$ and that with fixed current density $J_e = 1.0 \times 10^{12} A/m^2$ for the DMI constant ranging from $D = 0.0\ mJ/m^2$ to $D = 1.0\ mJ/m^2$, respectively. We find that there is a threshold current density (J_c) required to achieve field-free deterministic switching. However, if the current density is too high, DMI is not sufficient to create magnetization asymmetry leading to non-deterministic switching. This is similar to the case without DMI, and the in-plane field is too weak to make m_z deviate from 0. Also, DMI not only induces non-uniformity but also slows down the magnetization switching from the perpendicular to in-plane direction as indicated in Fig. 2(d). This is consistent with the results found in literature.[33,35] Our studies reveal that only appropriate values of the DMI constant can induce field-free reliable deterministic switching. Weak DMI is inadequate to induce the critical configuration. However, strong DMI can also lead to pulse-dependent instable magnetization dynamics as shown in Fig. 2(d) ($D = 1.0\ mJ/m^2$) due to the competition between SOT and DMI field destroying the conditions for deterministic switching. Hence, an optimum range of values for both current density and DMI is required to achieve field-free SOT switching. To seek a better understanding of the DMI-assisted SOT switching mechanism, we turn to energy analysis of our simulations.

Figure 3 shows the total energies as a function of the perpendicular magnetization component m_z corresponding to the various switching cases as shown in Figs. 1(b) and 2. For up-to-down switching, the magnetization starts from $m_z = +1.0$ and switches towards $m_z = -1.0$, and for down-to-up switching, the magnetization starts from $m_z = -1.0$ and switches towards $m_z = +1.0$. The filled dot on each curve indicates the point where the SOT is removed. Figure 3(a) shows the vastly different energy landscapes between DMI-induced and external-field-induced deterministic switching. For the external field case, the total energy increases monotonously within the SOT pulse, until the magnetization crosses into the negative position ($m_z < 0$), and eventually results in reversal once the pulse is terminated. However, in the DMI case, the change in the total energy within the SOT pulse is non-monotonous, and two states for $m_z > 0$ and $m_z < 0$ which are degenerate in energy [see also Figs. 3(c) and 3(d) for other current density and D] can exist. This may indicate why DMI induced field-free switching is unipolar in nature. In Fig. 3(b), we plot the total energy for both down-to-up and up-to-down switching for the cases shown in Figs. 2(a) and 2(b), respectively. The two curves are symmetric, and it shows that point A and point B are the same in energy.

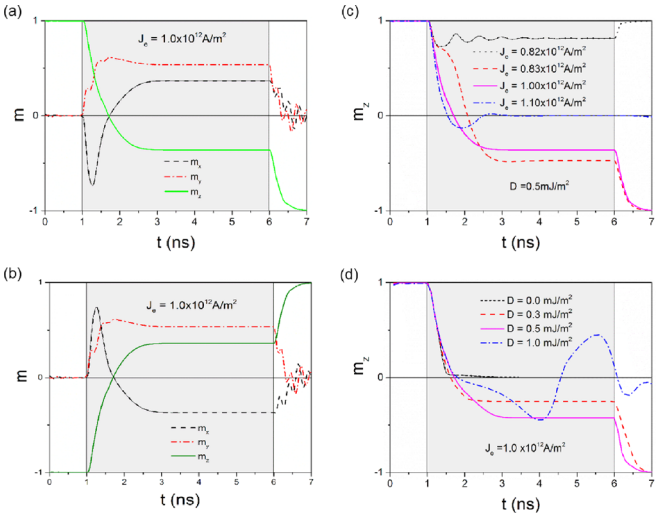

FIG. 2. Effect of current density and DMI constant variation on the switching performance for a device diameter of 100 nm (pulse is applied within the shaded region) with $\alpha = 0.1$: Temporal evolutions of x, y, z magnetization components for (a) up to down switching at a positive current density of 1.0×10^{12} A/m^2 and (b) down to up switching at a positive current density of 1.0×10^{12} A/m^2; Time domain plot of the perpendicular magnetization component for (c) various current densities at fixed $D = 0.5\ mJ/m^2$ and (d) various DMI constants at a fixed current density of 1×10^{12} A/m^2.

This indicates that it is the switching dynamics that determines the final state of the magnetization.[39,40] This is true for cases with or without the DMI. However, DMI induces intrinsic non-uniformity, resulting in degenerate energy states.

Next, we investigate the effect of geometrical modulation of the free layer on the DMI-SOT induced magnetization switching. We assume that the free layer is an ellipse with the long axis of Lx = 100 nm along the charge-current flowing direction (x-axis). The short axis is the spin polarization direction (y-axis) and is assumed to be Ly = 100 nm, 80 nm, and 60 nm. The temporal evolutions of perpendicular magnetization component m_z for different cases are plotted in Fig. 4: (a) DMI constant $D = 0.5\ mJ/m^2$ and current density $J_e = 1.0 \times 10^{12} A/m^2$ for various Lys; (b) DMI constant $D = 0.5\ mJ/m^2$ and Ly = 80 nm for various current densities; and (c) DMI constant $D = 0.5\ mJ/m^2$ and Ly = 60 nm for various current densities.

Figure 4(a) shows that the deterministic switching becomes unreliable if the aspect ratio (AR) is too high (e.g., Ly = 60 nm). The magnetization may switch back to its original state after the current is removed. Comparing Fig. 4(b) (Ly = 80 nm) with Fig. 2(c) (Ly = 100 nm), we see that the current density increases for shorter Ly. This can also be concluded from Fig. 4(c) (Ly = 60 nm) which shows that the minimum current density for the case of Ly = 60 nm has to be increased to $J_e = 1.3 \times 10^{12} A/m^2$ in order to achieve a reliable switching. This is due to the fact that larger AR induces a less effective shape anisotropy field along the spin polarization direction (y-axis) and thus increases the critical switching current densities J_c and reduces the switching stabilities.

Furthermore, we study the effect of the free layer geometry orientation on the switching performance. We assume that the free layer has an elliptical cross section of 100 nm × 60 nm and its long axis has an angle φ with the spin polarization direction, as shown in the subplot of Fig. 4(d). Hence, $\varphi = 90°$ corresponds to our previous case that the charge current flows through the HM along the long axis of the free layer. The temporal evolutions of perpendicular magnetization component m_z at various angle values are plotted in Fig. 4(d). We observe that when φ decreases from 90° to 67.5°, the switching becomes reliable and stable after the current is removed. However, further decreasing φ makes the switching harder, and it is unable to achieve a successful switching if φ is below 45° due to insufficient current

Published under license by AIP Publishing

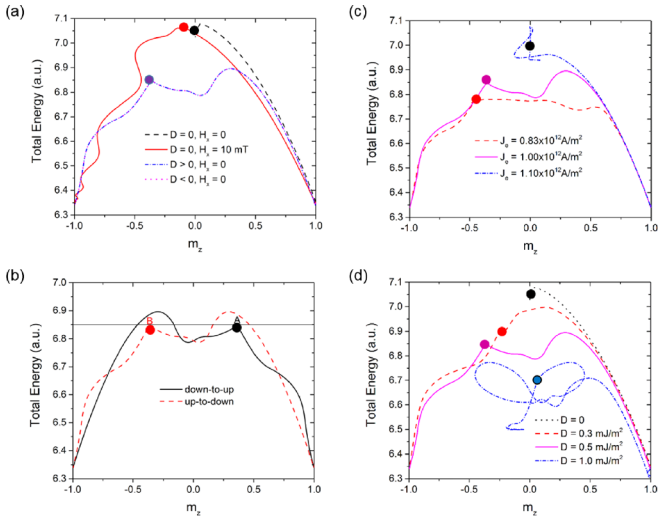

FIG. 3. Total energy as a function of perpendicular magnetization component m_z for various switching cases (the magnetization starts with $m_z = 1.0$ and switches towards $m_z = -1.0$. The dot on the curve is the point where SOT is removed): (a) total energy for switching cases depicted in Fig. 1(b) for a current density of 1.0×10^{12} A/m^2; (b) total energy for switching cases depicted in Fig. 2(a) (up-to-down) and 2(b) (down-to-up) for a positive current density of 1.0×10^{12} A/m^2 (A in the figure corresponds to the stable point within the pulse during down-to-up switching, and B in the figure corresponds to the stable point within the pulse during up-to-down switching); (c) total energy for switching cases depicted in Fig. 2(c) for various current densities at fixed D = 0.5 mJ/m^2; and (d) total energy for switching cases depicted in Fig. 2(d) for various DMI constants at a fixed current density of 1×10^{12} A/m^2.

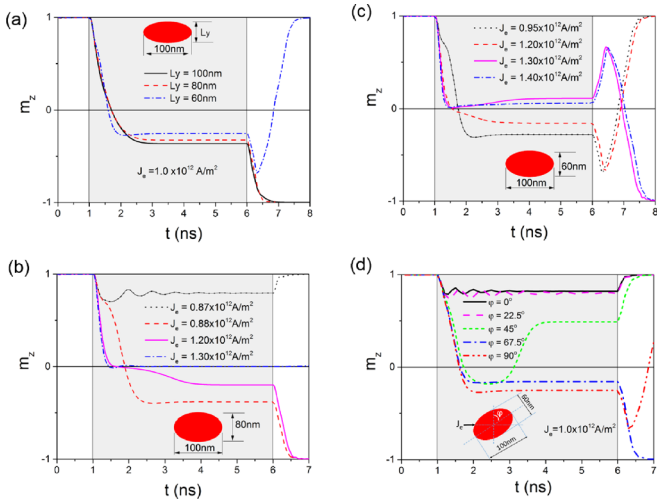

FIG. 4. Effect of geometric variations on the SOT switching performance for a fixed D = 0.5mJ/m^2 (the pulse is applied within the shaded region): temporal evolutions of magnetization components for (a) various Ly at fixed Je $= 1 \times 10^{12}$ A/m^2, (b) various current densities at Ly = 80 nm, (c) various current densities at Ly = 60 nm, and (d) various orientation angles between the major axis and the current direction at Ly = 60 nm and $J_e = 1.0 \times 10^{12}$ A/m^2.

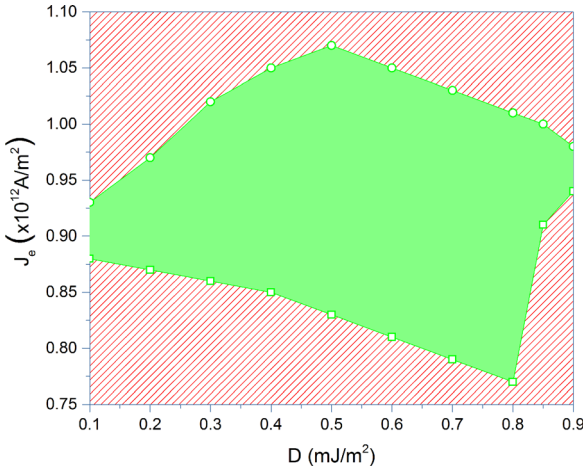

FIG. 5. Deterministic field-free spin-orbit torque switching window for varying DMI constants (D) and varying current densities (J_e) for a circular device of 100 nm diameter. The green region indicates where successful deterministic switching is observed.

densities. This means that higher J_c is required for a smaller φ angle. This may be due to the reason that for angles below 45°, the domain nucleates and propagates from an edge closer to the long axis of the ellipse instead of from the short axis and thus has a longer domain wall which needs higher SOT switching energies (see supplementary material). Here, we assume that the spin Hall angle remains constant for different orientations. We note that the switching performance in this case can be improved by using a larger damping constant and increasing the current densities (see supplementary material). This damping dependence is similar to the method of using the in-plane external field to assist the deterministic SOT switching.[39,41]

We also perform simulations with other DMI constants to further investigate the field-free deterministic switching performance. In Fig. 5, we map the current density window for deterministic switching at different DMI values ranging from D = 0.1 mJ/m^2 to D = 0.9 mJ/m^2 for a circular device of 100 nm diameter. We find a distorted diamond-shaped regime for deterministic switching bounded by the J_e vs. D curves. DMI values in the range of (0.5–0.8) mJ/m^2 are found to have the largest operating window for the applied current to achieve deterministic SOT switching. Our work can be applied immediately for experiments by tuning DMI strength through materials engineering. This tuning can be achieved by controlling either the ferromagnetic thickness or the spin-mixing conductance at the interface.[42] Interestingly, a larger spin-mixing conductance will also increase the damping in the system as required in our simulations.[43]

It should be noted that DMI induced field-free switching is for devices of intermediate size only. For devices with diameter <60 nm, the switching is coherent, DMI is unable to induce enough asymmetry to tilt the magnetization towards mz > 0 or mz < 0 within SOT, and hence, the switching is stochastic. For devices with diameter > 200 nm, we found that the magnetization is driven almost in-plane under high enough SOT, and the switching is not deterministic with thermal effects. A large in-

Published under license by AIP Publishing

plane field is needed to overcome the DMI effect in order for a successful switching.[17,40,44] Hence, the circular diameter of 100 nm is found to have the optimum geometry for maximizing the parametric window for deterministic switching. As in the case for different device sizes, we expect that the enclosed parametric window will decrease for an elliptical structure but may not necessarily exist in the same subset.

The results we have discussed so far are for simulations at zero temperature. For the purpose of practically realizing our proposed scheme, we need to consider thermal effects. We performed micromagnetic simulations at T = 100 K, 200 K, and 300 K. The temperature effect is included by adding a Langevin random field into the effective field in LLGS equation.[45] For each temperature, we performed 100 simulations in order to get the switching probabilities for fixed parameter combinations ($D = 0.5\ mJ/m^2$, $Je = 1.0 \times 10^{12}\ A/m^2$, and $t_p = 2$ ns). The switching probability is found to be 100%, 92%, and 83% at temperatures of 100 K, 200 K, and 300 K, respectively. These results show that the DMI induced field-free switching is robust against temperature (see supplementary material).

See supplementary material for the description of the LLG equations with DMI terms, the geometry effect, damping effect, and thermal effect on the switching.

This work was supported by A*STAR core fund and RIE2020 AME Core Fund Grant No. A1818g0042.

REFERENCES

[1]D. Apalkov, A. Ong, A. Driskill-Smith, M. Krounbi, A. Khvalkovskiy, S. Watts, V. Nikitin, X. Tang, D. Lottis, K. Moon, X. Luo, and E. Chen, ACM J. Emerging Technol. Comput. Syst. **9**, 1 (2013).
[2]L. Thomas, G. Jan, J. Zhu, H. Liu, Y. J. Lee, S. Le, R. Y. Tong, K. Pi, Y. J. Wang, D. Shen, R. He, J. Haq, J. Teng, V. Lam, K. Huang, T. Zhong, T. Torng, and P. K. Wang, J. Appl. Phys. **115**, 172615 (2014).
[3]M. Gajek, J. J. Nowak, J. Z. Sun, P. L. Trouilloud, E. J. O'Sullivan, D. W. Abraham, M. C. Gaidis, G. Hu, S. Brown, Y. Zhu, R. P. Robertazzi, W. J. Gallagher, and D. C. Worledge, Appl. Phys. Lett. **100**, 132408 (2012).
[4]Y. Huai, H. Gan, Z. Wang, P. Xu, X. Hao, B. K. Yen, R. Malmhall, N. Pakala, C. Wang, J. Zhang, Y. Zhou, D. Jung, K. Satoh, R. Wang, and L. Xue, Appl. Phys. Lett. **112**, 092402 (2018).
[5]J. Lourembam, B. Chen, A. Huang, S. Allauddin, and S. Ter Lim, Apply Phys. Lett. **113**, 022403 (2018).
[6]W. S. Zhao, Y. Zhang, T. Devolder, J. O. Klein, D. Ravelosona, C. Chappert, and P. Mazoyer, Microelectron. Reliab. **52**, 1848 (2012).
[7]G. Prenat, K. Jabeur, P. Vanhauwaert, G. Di Pendina, F. Oboril, R. Bishnoi, M. Ebrahimi, N. Lamard, O. Boulle, K. Garello, J. Langer, B. Ocker, M. C. Cyrille, P. Gambardella, M. Tahoori, and G. Gaudin, IEEE Trans. Multi-Scale Comput. Syst. **2**, 49 (2016).
[8]S. Fukami, T. Anekawa, C. Zhang, and H. Ohno, Nat. Nanotechnol. **11**, 621 (2016).
[9]C. F. Pai, L. Liu, Y. Li, H. W. Tseng, D. C. Ralph, and R. A. Buhrman, Appl. Phys. Lett. **101**, 122404 (2012).
[10]C. Bi, L. Huang, S. Long, Q. Liu, Z. Yao, L. Li, Z. Huo, L. Pan, and M. Liu, Appl. Phys. Lett. **105**, 022407 (2014).
[11]M. Cubukcu, O. Boulle, M. Drouard, K. Garello, C. O. Avci, I. M. Miron, J. Langer, B. Ocker, P. Gambardella, and G. Gaudin, Appl. Phys. Lett. **104**, 042406 (2014).
[12]L. Liu, O. J. Lee, T. J. Gudmundsen, D. C. Ralph, and R. A. Buhrman, Phys. Rev. Lett. **109**, 096602 (2012).
[13]I. M. Miron, K. Garello, G. Gaudin, P. J. Zermatten, M. V. Costache, S. Auffret, S. Bandiera, B. Rodmacq, A. Schuhl, and P. Gambardella, Nature **476**, 189 (2011).
[14]J. Cao, Y. Zheng, X. Su, L. Hao, Y. Wang, J. Bai, and F. Wei, Appl. Phys. Lett. **108**, 172404 (2016).
[15]O. J. Lee, L. Q. Liu, C. F. Pai, Y. Li, H. W. Tseng, P. G. Gowtham, J. P. Park, D. C. Ralph, and R. A. Buhrman, Phys. Rev. B **89**, 024418 (2014).
[16]G. Yu, P. Upadhyaya, K. L. Wong, W. Jiang, J. G. Alzate, J. Tang, P. K. Amiri, and K. L. Wang, Phys. Rev. B **89**, 104421 (2014).
[17]G. Yu, P. Upadhyaya, Y. Fan, J. G. Alzate, W. Jiang, K. L. Wong, S. Takei, S. A. Bender, L. Te Chang, Y. Jiang, M. Lang, J. Tang, Y. Wang, Y. Tserkovnyak, P. K. Amiri, and K. L. Wang, Nat. Nanotechnol. **9**, 548 (2014).
[18]M. Akyol, G. Yu, J. G. Alzate, P. Upadhyaya, X. Li, K. L. Wong, A. Ekicibil, P. Khalili Amiri, and K. L. Wang, Appl. Phys. Lett. **106**, 162409 (2015).
[19]L. You, O. Lee, D. Bhowmik, D. Labanowski, J. Hong, J. Bokor, and S. Salahuddin, Proc. Natl. Acad. Sci. **112**, 10310 (2015).
[20]S. Fukami, C. Zhang, S. Duttagupta, A. Kurenkov, and H. Ohno, Nat. Mater. **15**, 535 (2016).
[21]A. Van Den Brink, G. Vermijs, A. Solignac, J. Koo, J. T. Kohlhepp, H. J. M. Swagten, and B. Koopmans, Nat. Commun. **7**, 10854 (2016).
[22]Y.-C. Lau, D. Betto, K. Rode, J. Coey, and P. Stamenov, Nat. Nanotechnol. **11**, 758 (2016).
[23]I. Dzyaloshinsky, J. Phys. Chem. Solids **4**, 241 (1958).
[24]T. Moriya, Phys. Rev. **120**, 91 (1960).
[25]A. Cao, X. Zhang, B. Koopmans, S. Peng, Y. Zhang, Z. Wang, S. Yan, H. Yang, and W. Zhao, Nanoscale **10**, 12062 (2018).
[26]C.-Y. R. Lo Conte, G. V. Karnad, E. Martinez, K. Lee, N.-H. Kim, D.-S. Han, J.-S. Kim, S. Prenzel, and T. Schulz, AIP Adv. **7**, 065317 (2017).
[27]X. Ma, G. Yu, X. Li, T. Wang, D. Wu, K. S. Olsson, Z. Chu, K. An, J. Q. Xiao, K. L. Wang, and X. Li, Phys. Rev. B **94**, 180408(R) (2016).
[28]S. Meyer, B. Dupé, P. Ferriani, and S. Heinze, Phys. Rev. B **96**, 094408 (2017).
[29]N. Perez, E. Martinez, L. Torres, S. H. Woo, S. Emori, and G. S. D. Beach, Appl. Phys. Lett. **104**, 092403 (2014).
[30]J. Yu, X. Qiu, Y. Wu, J. Yoon, and P. Deorani, Sci. Rep. **6**, 32629 (2016).
[31]S. Li, S. Goolaup, J. Kwon, F. Luo, W. Gan, and W. S. Lew, Sci. Rep. **7**, 972 (2017).
[32]N. Mikuszeit, O. Boulle, I. M. Miron, K. Garello, P. Gambardella, G. Gaudin, and L. D. Buda-Prejbeanu, Phys. Rev. B **92**, 144424 (2015).
[33]J. Sampaio, A. V. Khvalkovskiy, M. Kuteifan, M. Cubukcu, D. Apalkov, and V. Lomakin, Appl. Phys. Lett. **108**, 112403 (2016).
[34]E. Martinez, L. Torres, N. Perez, M. A. Hernandez, V. Raposo, and S. Moretti, Sci. Rep. **5**, 10156 (2015).
[35]Y. Gao, Z. Wang, X. Lin, and W. Kang, IEEE Trans. Nanotechnol. **16**, 1138 (2017).
[36]M. J. Donahue and D. G. Porter, "OOMMF User's Guide Version 1.0," Interagency Report No. NISTIR 6376 (National Institute of Standards and Technology, Gaithersburg, MD, 1999).
[37]S. Rohart, A. Thiaville, and I. I. M. Framework, Phys. Rev. B **88**, 184422 (2013).
[38]S. Yan and Y. B. Bazaliy, Phys. Rev. B **91**, 214424 (2015).
[39]J. Park, G. E. Rowlands, O. J. Lee, D. C. Ralph, and R. A. Buhrman, Appl. Phys. Lett. **105**, 102404 (2014).
[40]W. Legrand, R. Ramaswamy, R. Mishra, and H. Yang, Phys. Rev. Appl. **3**, 064012 (2015).
[41]B. J. Chen, S. Ter Lim, and M. Tran, IEEE Magn. Lett. **7**, 3105205 (2016).
[42]X. Ma, G. Yu, C. Tang, X. Li, C. He, J. Shi, K. L. Wang, and X. Li, Phys. Rev. Lett. **120**, 157204 (2018).
[43]J. Lourembam, A. Ghosh, M. Zeng, S. K. Wong, Q. J. Yap, and S. Ter Lim, Phys. Rev. Appl. **10**, 044057 (2018).
[44]M. Baumgartner, K. Garello, J. Mendil, C. O. Avci, E. Grimaldi, C. Murer, J. Feng, M. Gabureac, C. Stamm, Y. Acremann, S. Finizio, S. Wintz, J. Raabe, and P. Gambardella, Nat. Nanotechnol. **12**, 980 (2017).
[45]B. Chen, T. Zhou, S. Y. Sim, S. Ter Lim, and H. Gong, Phys. Lett. A **382**, 3429 (2018).

Published under license by AIP Publishing